www.ijecs.in
International Journal Of Engineering And Computer Science ISSN:2319-7242
Volume 4 Issue 6 June 2015, Page No. 12766-12773

Anatomization of Medical Image Segmentation with Novel Proposal

Nagaraja G[1] G.Pradeep Reddy[2]

[1]Research Scholar, Shri Venkateshwara University,
Gajroula, UP

[2]Asst.Professor, ECE Department, Gokaraju Rangaraju Institute of Engineering and Technology,Bachupally,Telangana

In this article we introduce a novel variational model for two-phase segmentation tasks, which is related to the popular Chan-Vese(CV) segmentation model[4]. In particular, the proposed model is based on a *discriminant analysis* of the given data. Level set methods are used to realize this approach is numerically. We start by applying CV model on medical ultrasound data perturbed by multiplicative speckle noise. The respective observations are noted i.e. Section1. Subsequently, discriminant analysis based segmentation model is applied i.e. in Section2.Finally, we validate the methods on real patient data from echocardiographic examinations in Section3.

1 Objective

Standard segmentation formulations such as the popular CV approach, tend to produce L^2 data fidelity term in the Inapplicability of the ICC for US imaging. By incorporating physical noise models like additive Gaussian, Loupas and the Rayleigh in segmentation algorithms the robustness and segmentation accuracy can be increased significantly. This adaption leads in general to increased computational effort, due to sophisticated modeling and relatively complex numerical solving schemes Numerical Realization (minimization problem) with additional parameters to be optimized. The aim is to increase the robustness of medical US data by introducing a simple variational segmentation formulation which accounts for the impact of multiplicative speckle noise. Simultaneously, we aim to obtain closed segmentation contours which delineate the endocardial border of the left ventricle, as this is not possible with the proposed variational segmentation framework due to the global convex segmentation approach in Numerical Realization (minimization problem).

To give a motivation for the proposed approach, we observe the impact of two different noise models on an *intensity histogram*, i.e., additive Gaussian noise (1) and multiplicative speckle noise as modeled(3) in

The perturbation with white noise during the image formation process is modeled as,

$$f = u + \eta \qquad (1)$$

for which η is a normal distribution random variable with mean 0 and variance σ^2 , i.e., the probability density function of η is given by ,

$$p(\eta) = \frac{1}{\sqrt{2\pi}\sigma} e^{-\frac{\eta^2}{\sigma^2}}.$$

from (1), it is clear that this form of noise is signal-independent and has a globally identical distribution of noise.

The Loupas noise model originates form an experimentally derived model for multiplicative speckle noise by Tur, Chin and Goodman in [15]. The image formation process is given by ,

$$f = u + u^{\frac{\gamma}{2}}\eta \qquad (2)$$

This special case is known as Loupas noise model and image formation process[26 §1].

$$f = u + \sqrt{u}\eta \qquad (3)$$

The effect of additive Gaussian noise is illustrated in Figure 1a. Obviously, for a fixed variance $\sigma^2 > 0$ there is a globally identical impact on the signal distribution. This is natural, since additive Gaussian noise is signal-independent [2].

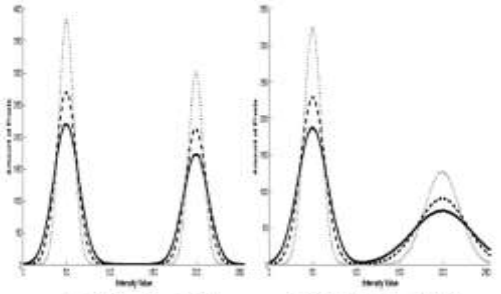

(a) Additive Gaussian Noise (b) Multiplicative Speckle Noise

Fig1. *Effect of additive and multiplicative noise on the intensity distribution in an image histogram*

For multiplicative speckle noise one can observe different characteristics in Figure 1b. In regions with high intensity

values the grayscale distribution gets spread out much wider than in regions with low intensity values. This effect is amplified for increasing noise variance σ^2. Thus, it is more difficult to separate the two signal distributions compared with additive Gaussian noise, especially in the overlapping areas of the histogram. It is our goal to incorporate this observation on the signal distribution in US images efficiently for a robust segmentation of US images.

CV method Restrictions

In the following we discuss the characteristics of the Chan-Vese formulation [4] for the situation of images perturbed by multiplicative speckle noise as illustrated in Figure 1b.

In order to overcome the enormous numerical effort of using an explicit parameterization of Γ, Chan and Vese propose in [4] to express E_{cv} in with the help of level set functions. Until today a huge variety of applications for level set methods have been proposed, e.g., classical segmentation tasks [4,12,13,14], simulation and modeling [17], and rendering [18]. They use a signed distance function $\Phi : \Omega \rightarrow R$ as introduced in [4] such that the segmentation contour Γ and the two respective regions are given implicitly as level sets of Φ.

Using the notation above, the energy functional in *CV segmentation model* [4] can be rewritten in the context of *level set methods* as,

$$\begin{aligned} F_{cv}(c_1, c_2, \Phi) = \lambda_1 \int_{\Omega} \left(c_1 - f(\vec{x})\right)^2 H(\Phi)\, d\vec{x} \\ + \lambda_2 \int_{\Omega_2} \left(c_2 - f(\vec{x})\right)^2 (1 - H(\Phi(\vec{x})))\, d\vec{x} \\ + \beta \int_{\Omega} \delta_0(\Phi(\vec{x})) |\Delta\Phi(\vec{x})|\, d\vec{x} + \\ \gamma \int_{\Omega} H(\Phi(\vec{x}))\, d\vec{x} \end{aligned} \tag{4}$$

and the associated minimization problem reads as,

$$inf\{F_{cv}(c_1, c_2, \Phi) |\, c_i\, constant,\ \ \Phi \in w^{1,1}(\Omega)\}. \tag{5}$$

In general, a proof for existence of minimizers for (5) is hard to obtain, due to the non-convexity of (4). However, using the results from *convex relaxation* discussed in [16] , the authors Brown, Chan and Bresson prove the existence of global optima for the relaxed problem in [3].

In most segmentation tasks it is not reasonable to penalize the size of the segmentation area and hence the respective regularization term is disregarded [4], i.e., formally $\gamma = 0$ in (4). We follow this approach and discuss a reduced variant of the original Chan- Vese formulation in the following.

To compute a local minimum for (5), an *alternating minimization scheme* is used as indicated in [4]. Thus, the minimization problem (5) is transformed into two decoupled minimization problems, i.e.,

$$inf\{F_{cv}(c_1, c_2, \Phi^n) |\, c_i\, constant\ \}, \tag{6a}$$
$$inf\{F_{cv}(c_1^{n+1}, c_2^{n+1}, \Phi)\ \Phi \in w^{1,1}(\Omega)\}. \tag{6b}$$

To solve (6a), the optimal constants c_1 and c_2 can be computed for a fixed Φ analogously to [19] as mean values of the respective sub regions $\Omega_1, \Omega_2 \subset \Omega$ using [1].

For the minimization of the subsequent *minimal partition problem* (6b) the authors in[4] propose to use regularized versions of the Heavyside function H and the one dimensional $\delta -$ Dirac measure δ_0 , i.e., for a small $\epsilon > 0$ they use the following functions,

$$\begin{aligned} H_\epsilon(x) &= \frac{1}{2}\left(1 + \frac{2}{\Pi}\, arctan\left(\frac{x}{\epsilon}\right)\right), \quad \delta_\epsilon(x) \\ &= H'_\epsilon(x) = \frac{1}{\Pi\left(\frac{x^2}{\epsilon} + \epsilon\right)} \end{aligned} \tag{7}$$

Denoting with $f(x, u, \xi) = f(x, \Phi, \nabla\Phi)$ the integrand of F_{cv} and using the regularized functions in (7), the strong formulation of the *Euler-Lagrange equation* for minimization of (6b) with respect to Φ can be deduced as,

$$\begin{aligned} 0 &= \sum_{i=1}^{n} \frac{\partial}{\partial x_i}\left[f_{\xi_i}(x, u, \xi)\right] \\ &\quad - f_u(x, u, \xi) \\ &= \delta_\epsilon\left(\Phi(\vec{x})\right)\left(\beta div\left(\frac{\nabla\Phi(\vec{x})}{|\nabla\Phi(\vec{x})|}\right)\right. \\ &\quad - \lambda_1 (f(\vec{x}) - c_1)^2 \\ &\quad \left. + \lambda_2 (f(\vec{x}) - c_2)^2\right), \end{aligned} \tag{8}$$

with the Cauchy boundary condition [4],

$$\frac{\delta_\epsilon(\Phi(\vec{x}))}{|\nabla\Phi(\vec{x})|} \frac{\partial\Phi}{\partial\vec{n}}(\vec{x}) = 0 \text{ for all } \vec{x} \in \partial\Omega,$$

which has to be fulfilled by any minimizer $\widehat{\Phi}$ of (6b) a.e. on the domain Ω. Introducing an artificial temporal variable $t \in R^{\geq 0}$ and applying a gradient descent approach, one is interested in a *stationary solution* of the resulting PDE, i.e., $\frac{\partial\Phi}{\partial t} = 0$ for (8). A forward Euler time discretization can be applied as discussed in *numerical realization* [16]. and hence one gets the following iterative update. We exchange the regularized δ- Dirac measure δ_ϵ by $|\nabla\Phi^n|$ to expand the evolution of Φ to all level sets (cf. Level Set Methods [16]), i.e., globally on Ω. Then the iterative update reads as,

$$\begin{aligned} &\Phi^{n+1}(\vec{x}) \\ &= \Phi^n(\vec{x}) \\ &+ \Delta t |\nabla\Phi^n(\vec{x})| \left(\beta\, div\left(\frac{\nabla\Phi^n(\vec{x})}{|\nabla\Phi^n(\vec{x})|}\right)\right. \\ &\left. - \lambda_1 (f(\vec{x}) - c_1)^2 + \lambda_2 (f(\vec{x}) - c_2)^2\right), \end{aligned} \tag{9}$$

This can be interpreted as motion in *normal direction* controlled by both internal (mean curvature) and external forces (data fidelity) as discussed in Choice of velocity field V [16]. The curvature term in (9) can be approximated using spacial discretization of parabolic terms[16] as introduced in Numerical Realization[16].

For this case the stability of the iterative update $\Phi^n \rightarrow \Phi^{n+1}$ is guaranteed for the *associated convection-diffusion* PDE [20, §6.4] by the Courant-Friedrich-Lewy condition

using Theorems Convergence for normal velocity [20,Theorem 6.3.1] and Convergence for mean curvature velocity [20, Theorem 6.3.1],

$$\Delta t \max_{\vec{x}\in\Omega} \left\{ \sum_{i=1}^{n} \frac{|D(c_1, c_2, f)(\vec{x}) \Phi x_i(\vec{x})|}{|\nabla \Phi(\vec{x}) \Delta x_i|} + \frac{2\beta}{(\Delta x_i)^2} \right\} < 1, \quad (10)$$

for which $D(c_1, c_2, f)(\vec{x}) = \lambda_2 (f(\vec{x}) - c_2)^2 - \lambda_1 (f(\vec{x}) - c_1)^2$ denotes the data fidelity.

The alternating minimization scheme for the level set formulation of the Chan-Vese functional is summarized in CV Segmentation Algorithm[25]. Note that we introduced a second index M for the *maximal number of inner iterations* until the (optional) reinitialization of Φ to a signed distance function as described in *Numerical Realization*[16].

Keeping the optimal constants c_1, c_2 fixed and disregarding the smoothness term for Φ, i.e., formally $\beta = 0$, we observe that the data fidelity term in (4) gets minimal, if all intensity values with respect to the mean values of Ω_1 *and* Ω_2. Hence, a pixel gets assigned to Ω_2, if the difference of its intensity value to the respective mean value is smaller than to the mean value of the background region (and vice versa).

Obviously, this induces a *classification threshold*

$$t_{cv} = \frac{c_1 + c_2}{2}.$$

Note that this threshold only depends on the mean values of the two signal distributions and does not consider the respective *variances*. As discussed in [16] L^2 data fidelity term and hence the induced threshold t_{cv} represent an optimal choice for segmentation tasks on images perturbed by additive Gaussian noise. This can also be seen in Figure 1a, where the noise perturbation is *global* and an optimal threshold only depends on the mean values of the respective signal distributions.

However, this model is rather inapplicable for images perturbed by multiplicative noise. This fact is illustrated in Figure 2. The two solid black lines resemble the intensity values of an unbiased signal u in an image intensity histogram. By adding multiplicative speckle noise according to (3) with
γ=1and noise variance parameter σ^2 = 2.7 we generated a perturbed image f. As can be seen at the image intensity histogram of f (dashed line), the intensity values get spread out according to a local normal distribution induced by the normal distributed random variable η in (3). Due to the multiplicative nature of this noise from the noise variance is significantly higher in the part with higher intensity values of the image histogram. Thus, it is more challenging to separate the two signals, especially in the overlapping part of the histogram.

The red line in Figure 2 illustrates the threshold t_{cv} induced by the mean values of the two signals (black solid lines). Apparently, the data cannot be partitioned reasonably by t_{cv} and a shift to the left side of the histogram would be appropriate. In Section 2 we introduce a method to estimate a threshold by the means of *discriminant analysis* that also considers the variance of the two signal distributions and hence leads to a better partitioning of the signal intensities (indicated by the blue dashed line).This observation of the induced threshold t_{cv} gets even more apparent, if one recalls the Euler-Lagrange equations (8) of the minimal partition problem (6b). By setting $\lambda_1 = \lambda_2$ (standard parameter choice in [4]) the associated Euler-Lagrange equations with respect to the level set function Φ are given by,

$$0 = \delta_\epsilon(\Phi(x)) \left(\mu \, div\left(\frac{\nabla \Phi(x)}{|\nabla \Phi(x)|} \right) - (f(x) - c_1)^2 + (f(x) - c_2)^2 \right)$$

$$= \delta_\epsilon(\Phi(x)) \left(\mu \, div\left(\frac{\nabla \Phi(x)}{|\nabla \Phi(x)|} \right) - 2(c_2 - c_1) \left(f(x) - \underbrace{\frac{c_1 + c_2}{2}}_{= t_{cv}} \right) \right).$$

Here, μ is the rescaled parameter β in (8). Disregarding the regularization term for Φ, i.e., $\mu = 0$, it gets clear that the Euler-Lagrange equation only holds in one case.

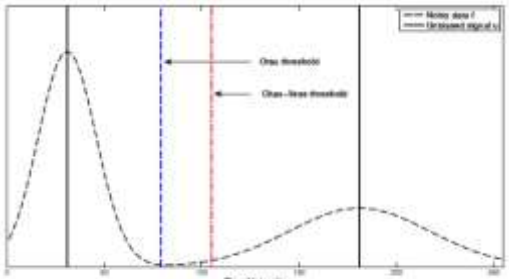

Fig.2. *Comparison of the Chan-Vese threshold t_{cv} and the Otsu threshold t_o (discussed in Section 2) in the presence of multiplicative noise.*

The equilibrium status of the evolution of Φ is obtained, if the segmentation contour is situated at points $\vec{x} \in \Omega$ for which $f(\vec{x}) = t_{cv}$ holds true (see also [16, §12.2]). For the case $\lambda_1 \neq \lambda_2$, the two L^2 terms are not weighted equally and hence the induced threshold is shifted towards the mean value with higher regularization parameter. Note that it is in general difficult to choose the two parameters λ_1, λ_2 appropriately for a given data set (see discussion below). Hence, in most cases the two parameters are chosen equally for the sake of simplicity [4].

As we show in Section 3 the data fidelity term of the Chan-Vese model (4) and the induced threshold t_{cv} are not appropriate for medical ultrasound images and lead to erroneous segmentation results.

The main drawback of the classical Chan-Vese formulation (4) is the non-convexity of the associated energy functionals and consequently the existence of local *minima*, which lead to unsatisfactory segmentation results. This is due to two different facts. First, the original Chan-Vese formulation in [4] has *four different parameters* to be chosen for a given data set. Disregarding the regularization term for the segmentation area, i.e., γ = 0,, three parameters have to be

estimated for a given data set. Since these parameters influence each other, this leads to many local minima in the parameter space. Obviously, the optimization of these parameters for a huge set of images to be segmented is very time consuming, and hence a more simple model with less parameters would be advantageous in such a situation.

The second reason for the existence of local minima is based on the fact that a solution of the minimization problem (5) can only be achieved by an alternating minimization scheme of the two corresponding sub problems (6a) and (6b), as realized in CV Segmentation Algorithm[25]. Obviously, there is a strong dependence between Φ and the optimal constants C_1 and C_2 ,since the estimation of optimal constants C_1 and C_2 depends on the current state of Φ and vice versa. This alternating minimization frequently converges to a local minimum, depending on the specified parameter set. For fixed parameters λ_1, λ_2 and β this local minimum depends on the specific initialization of Φ and thus of the segmentation contour Γ, since CV Segmentation Algorithm[25] is totally deterministic.

As can be seen in two slightly different situations in Figure 3, the success of the Chan-Vese segmentation crucially depends on the chosen initialization of the segmentation contour Γ. The red rectangle in Figure 3a shows the first initialization within the dark region of the left ventricle in an US B-mode image of the human heart in an apical four-chamber view. Since only few pixels inside the rectangle do not belong to the background region, the Chan-Vese method converges to an acceptable segmentation of the LV as shown in Figure 3b.

However, if the initialization is slightly changed, one obtains totally different segmentation results as illustrated in Figure 3d, in which a part of the septal wall is segmented. For this result, a shift of the previous initialization one pixel to the left has been performed. The reason for this unsatisfying segmentation result is that some bright pixels in the initialization in Figure 3c lead to the estimation of a high mean value within this region. Although most pixels within the segmentation contour belong the background, the iterative optimization process converges to this local minimum.

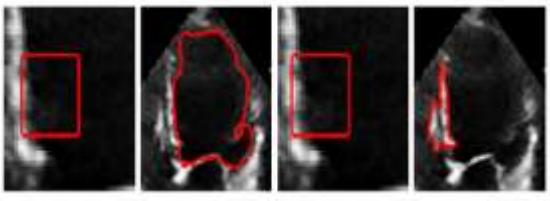

(a) 1st Initialization (b) CV result for (a) (c) 2nd Initialization (d) CV result for (c)

Fig.3. *The problem of local minima illustrated by segmentation results of the Chan-Vese (CV) model based on two slightly different initialization.*

These observations motivate us to propose a novel segmentation formulation in Section2 that overcomes the problems discussed above, e.g., the strong dependence of the obtained segmentation results on the chosen initialization of the segmentation contour
as discussed above.

2 Segmentation Prototype established by suggested Discriminant Analysis

In order to overcome the drawbacks of the popular Chan-Vese segmentation model discussed in Section 1 we propose a novel variational segmentation formulation based on level set methods. This section represents an extended version of the work proposed in [11]. The data fidelity term of the Chan-Vese formulation is exchanged by a *simple* term, which partitions the data according to an optimal threshold by means of discriminant analysis. We demonstrate its advantages in terms of *robustness* and *efficiency* and discuss a numerical realization to segment medical ultrasound images. Finally, we show its superiority over the Chan-Vese method on real patient data from echocardiographic examinations.

Discriminant Analysis for calculating Optimal Threshold

To challenge the problem of misclassification of pixels due to multiplicative noise (cf. Section 1), we propose to use an established statistical approach to find an optimal threshold t_0. In this context, optimal refers to determining a threshold that minimizes the within-class variance and maximizes the between-class variance between two classes of pixels simultaneously. The idea is to apply discriminant analysis from statistics on an image histogram and subsequently determine the optimal threshold. This approach corresponds to the popular *Otsu thresholding method* in [9] for grayscale images.

Let us denote the number of pixels of a given grayscale image *f* with *N* and let

$$H: N^{256} \rightarrow [0,1]$$

be the *normalized histogram* of this image. Then, the intraclass variances of C_0 and C_1 are given by,

$$\sigma_0^2(t) = \sum_{i=0}^{t} p_i\big(i - m_0(t)\big)^2, \quad \sigma_1^2(t) = \sum_{i=t+1}^{255} p_i\big(i - m_1(t)\big)^2. \tag{11}$$

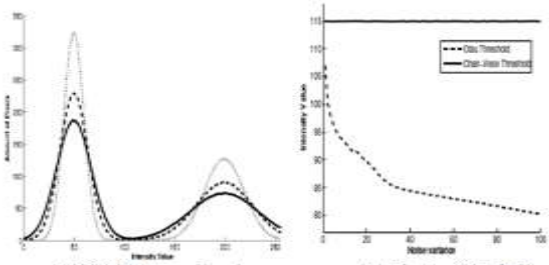

(a) Multiplicative speckle noise (b) Adaption of thresholds

Fig. 4. *Effect of noise variance σ^2 on an image histogram in (a) and the adaption of the Otsu threshold t_0 compared to the Chan-Vese threshold t_{cv} in (b).*

Based on the intraclass variances in (11), one can define the global within-class variance σ_W and the between-class variance $\sigma_B$by,

$$\sigma_W(t) = P_0\sigma_0^2(t) + P_1\sigma_1^2(t), \tag{12a}$$

$$\sigma_B(t) = P_0\,(m_0(t) - m)^2 + P_1\,(m_1(t) - m)^2, \tag{12b}$$

where $P_0 = \sum_{i=0}^{t} p_i$ and $P_1 = \sum_{i=t+1}^{255} p_i$ represent the relative portions of the respective classes. Finally, the optimal Otsu threshold t_0 can be computed by maximizing,

$$t_0 = \underset{0 \le t < 255}{argmax} \frac{\sigma_B(t)}{\sigma_W(t)} \quad (13)$$

Maximizing the fraction in (13) corresponds to finding a threshold t, which induces an optimal relation of small within-class variance and large between-class variance. In particular, Otsu shows in [9] that minimizing σ_w and maximizing σ_B can be achieved simultaneously (because $\sigma_w + \sigma_B$ equals to the overall variance of the image).

Figure 4a shows the impact of multiplicative speckle noise on an image histogram according to the noise model in (3) with increasing noise variance σ^2. In Figure 4b one can see how the Otsu threshold t_0 is adapted with increasing noise variance. As already discussed in Section1, signals with high intensity values get spread much higher due to the multiplicative nature of speckle noise and hence the threshold t_0 shifts to the left side of the histogram in Figure 4a, i.e., the value of t_0 in Figure 4b decreases. In contrast to that, the threshold t_{cv} induced by the Chan-Vese model (cf. Section 1) stays constant for increasing noise variance σ^2, since it depends only on the mean values of the respective signal distributions.
In addition, Figure 2 illustrates that the threshold σ^2 (blue line) separates the two signal distributions significantly better than the Chan-Vese threshold
σ^2 (red line). This leads to less misclassification of intensity values for medical ultrasound images. Therefore, we incorporate the threshold t_0 derived from discriminant analysis into a novel variational segmentation formulation in the following.

Proposed variational segmentation model

Motivated by the observations in Section 1 and using the optimal threshold t_0 derived from the discriminant analysis discussed above, we introduce a novel variational segmentation formulation for medical ultrasound images in the following. Using the notation from Section 1 the proposed segmentation model reads as,

$$\begin{aligned} &E(\Phi) \\ &= \frac{1}{2}\int_{\Omega} sgn\big(\Phi(\vec{x})\big)(f(\vec{x}) - t_0)d\vec{x} \\ &+ \beta\int_{\Omega} \delta_0\big(\Phi(\vec{x})\big)|\nabla\Phi(\vec{x})|\overrightarrow{dx}\,. \end{aligned} \quad (14)$$

The idea of the model in (14) is to partition the given data according to the optimal threshold t_0 introduced above using a *linear distance* measure. Analogously to the Chan-Vese model, we enforce *smoothness* of the level set function Φ by minimizing its total variation at the segmentation contour Γ. Since the threshold t_0 is fixed throughout the segmentation process, one only has to minimize with respect to Φ, i.e., one has to solve a *minimal partition problem*,

$$\inf\{E(\Phi)|\Phi \in W^{1,1}(\Omega)\}. \quad (15)$$

Note that the proposed model in (14) is not restricted on ultrasound data since it does not explicitly model the noise perturbation as done, e.g., in Variational segmentation framework for region-based segmentation[1]. Furthermore, it can also be easily extended to multiphase segmentation problems (cf. [12,9]).

3 Results

In this section we validate the proposed method from Section 2 on eight different 2D US B-mode data sets from real examinations of the human heart imaged with a Philips iE33 ultrasound system in different views, i.e., two-chamber, three-chamber, and apical four-chamber views. We use this data, to demonstrate that it is possible to use the proposed model for heterogeneous data from echocardiography. The segmentation task for these images is to delineate the endocardial border of the left ventricle as echocardiographic experts would perform it during their manual measurements.

We compare the proposed model qualitatively and quantitatively with the traditional Chan-Vese model from Section1 with respect to robustness, efficiency, and accuracy of the respective segmentation algorithms .

Qualitative comparison

To compare the traditional Chan-Vese segmentation method (CV Segmentation Algorithm[25]) with the proposed segmentation method (Algorithm 3), we tested a huge range of parameters for the two implementations, i.e.,

- maximum number of inner iterations until reinitialization M ∈ [5, 5000] ,
- smoothness parameter $\beta \in [1, 2200]$,
- data fidelity weights for the Chan-Vese algorithm $\lambda_1, \lambda_2 \in [0.5, 1.5]$.

During our experiments we observed a significantly higher robustness in terms of parameter choice for the proposed model in Section 2. While the proposed method gave satisfying results for many parameter setups within the sampled range, the Chan-Vese method converged only for a few parameter settings to reasonable segmentation results. Furthermore, these feasible parameter setups could not be located in a close range, but were spread over the whole parameter space. In contrast to that we could observe a good correlation between the parameters β and M for the proposed method, i.e., we found the best segmentation results when the maximum number of inner iterations until reinitialization of Φ was chosen as $M \in [\frac{\beta}{2}, \frac{3\beta}{2}]$. This observation is constituted by the choice of the temporal step width Δt with respect to the CFL stability condition (16).

$$\Delta t \underset{\vec{x}\in\Omega}{max}\left\{\sum_{i=1}^{n} \frac{\left|D(t_0,f)(\vec{x})\Phi_{x_i}(\vec{x})\right|}{|\nabla\Phi(\vec{x})|\Delta x_i} + \frac{2\beta}{(\Delta x_i)^2}\right\} < 1, \quad (16)$$

for which $D(t_0, f)(\vec{x}) = f(\vec{x}) - t_0$ denotes the data fidelity term.

Note that choosing the maximum number of inner iterations M too high leads to unwanted topological changes and an expansion of the segmentation contour over anatomical structures in regions of low contrast (e.g., apical part and

mitral valve of left ventricle in Figure 5). Thus, frequent reinitialization is recommended for level set segmentation of medical ultrasound data. We could observe that the standard parameter choice $\lambda_1 = \lambda_2$ for the Chan-Vese method is suboptimal for medical ultrasound images. This is reasonable, due the impact of multiplicative speckle noise as discussed in Section1. However, if we selected these two parameters such that their ratio was $\lambda_1 = \lambda_2 < 0.7$, we could observe that the labels of the sub regions Ω_1 and Ω_2 tend to switch during the evolution process of Γ. Thus, for these parameter settings we were not able to perform a segmentation of the cavum of the left ventricle, but only for the tissue of the myocardium.

As already indicated in Section 1 the traditional Chan-Vese method is in general prone to convergence to unwanted local minima. Due to the interconnection of the two sub problems in (6a,6b), the result of the alternating minimization strongly depends on the *initialization* of Φ.

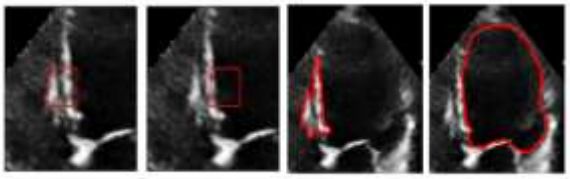

(c) 1st Initialization at septal wall of LV (d) 2nd Initialization in cavum of LV (e) CV Segmentation for (a) and (b) (f) Our segmentation for (a) and (b)

Fig.5. *Different initializations of Γ within an US B-mode image of the left ventricle (LV) of a human heart and the respective segmentation results of the CV model and the proposed model.*

As illustrated in Figure5 the proposed method is very robust in terms of initialization, due to the fact than one only has to solve a minimal partition problem and thus avoids unwanted local minima. In Figure 5a and 6b we show two different initializations of the segmentation contour Γ at the septal wall and in the cavum of the left ventricle, respectively. Both initializations lead for the Chan-Vese method to a local segmentation of the septal wall tissue (bright region) as can be seen in Figure 5c. While this is reasonable for the first initialization, the result for the second initialization is unwanted, since most pixels in the inside region of Γ belong to the dark background. The proposed method on the other hand leads in both cases to the same segmentation in Figure 5d, which delineates the inner contour of the left ventricle as required. In order to segment the myocardial tissue similar to Figure 5c, one has to invert the sign of Φ during its initialization as discussed in Section2.

Data Fidelity of both models i.e. Chan-Vese formulation (4) and the proposed model (14) for real US B-mode images from a human left ventricle (LV) in an apical four-chamber view. We can infer this by going through figures 6(a) to 6(f).

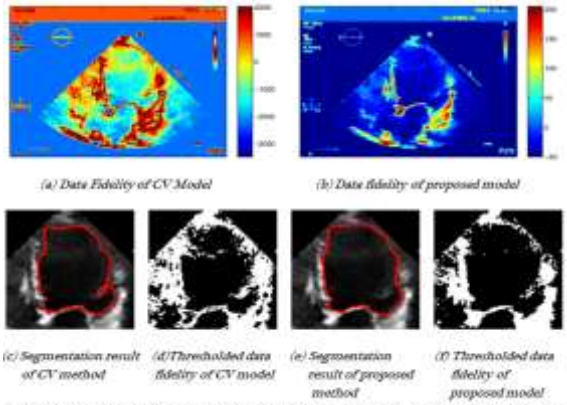

(a) Data Fidelity of CV Model (b) Data fidelity of proposed model

(c) Segmentation result of CV method (d) Thresholded data fidelity of CV model (e) Segmentation result of proposed method (f) Thresholded data fidelity of proposed model

Fig.6. *Direct comparison of data fidelity and segmentation results for the CV model and the proposed model.*

To observe this last fact even better, we show the thresholded data fidelity terms to indicate pixels with non-negative value (white pixels) and negative value (black pixels) of the Chan-Vese model and the proposed model in Figure 6d and 6f, respectively. As can be clearly seen, the speckle noise artifacts in the upper left and lower right part of the cavum have a less severe impact on the data fidelity of the proposed method compared to the Chan-Vese model. This leads to a more robust and accurate segmentation performance as we show in quantitative measurements [11§4.5].

Dataset	1	2	3	4	5	6	7	8
Observer variability	0.9217	0.9285	0.8906	0.8994	0.9003	0.9348	0.9301	0.9414
Chan-Vese model	0.8731	0.9075	0.7551	0.9278	0.8229	0.7551	0.8874	0.8942
Proposed model	0.8803	0.9443	0.8132	0.9254	0.8401	0.8172	0.8934	0.9191

Table 1. *Dice index values for comparison with manual segmentation*

Proposed model limitation

Chan-Vese and proposed models cannot be used universally for segmenting of medical US images because they are *low-level segmentation* methods, i.e., segmentation only based on image intensities, they lead to erroneous segmentation results in specific situations. Problems can occur when the data is heavily perturbed or can lead to missing anatomical structures during suboptimal condition.
Hence, any low-level segmentation algorithm would also segment misleadingly connected regions.Figure7 gives two examples for the limit of the proposed segmentation model. Due to the perturbation, the segmentation contour expands out of the left ventricle and leads to an unsatisfying segmentation result[Figure 7a].

US imaging in a *suboptimal angle*[Figure 7b] of an apical four-chamber view of the left ventricle. Here, no shadowing effects occur and all endocardial contours give a relatively high contrast for segmentation. However, due to a suboptimal imaging plane, the mitral valve (center bottom of image) is only imaged partly and thus does not appear to be closed. This leads eventually to a segmentation of the connected

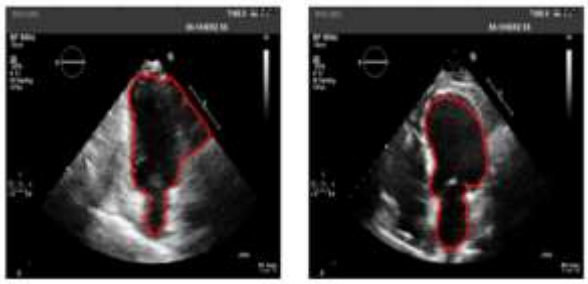

(a) Erroneous segmentation result due to shadowing effects

(b) Erroneous segmentation result due to missing anatomical structures

Fig.7. Erroneous segmentation results of the proposed method due to missing anatomical structures and shadowing effects illustrate the limits of this model.

left atrium by mistake. Note that this problem also arises even for high values of the smoothness parameter β in (13).

In order to successfully segment medical ultrasound images that suffer from the two problems indicated above, one needs additional information about the data.

4 Analysis

We proposed a novel variational model for two-phase segmentation tasks in this section. Motivated by the problems arising for the traditional Chan-Vese model, when applied for medical ultrasound data, we deduced a segmentation formulation that accounts for the characteristics of multiplicative speckle noise, while simultaneously reducing the complexity of the problem formulation. On a direct comparison of both algorithms for real patient data from echocardiographic examinations we observed that the proposed method performs significantly better in terms of robustness and segmentation accuracy than the Chan-Vese method and achieved a higher average Dice index when compared with manual delineations from experienced physicians.

The reason for this improvement is the incorporation of an optimal threshold by means of discriminant analysis, which also respects the signal-dependent noise variance of the image intensity distributions. Additionally, the use of a linear distance measure, in contrast to the common L^2 data fidelity term of the Chan-Vese model, further increases the robustness under outlier pixels. For the globally optimized parameter settings the Chan-Vese method performed better in terms of computational effort. However, in general both methods show similar run-times since CV Segmentation Algorithm[25] and 3 have a analogous structure. Finally, we investigated typical cases for which both models are not feasible and lead to erroneous segmentation results. This motivates the incorporation of further a-priori knowledge of the data, e.g., shape information.

Although we tested both segmentation algorithms from this section on real 3D US data of the human heart captured with a X11 transducer of a Philips iE33 imaging system, we could only observe a marginal improvement in the segmentation results using the proposed segmentation model. We suppose that this observation is due to the different imaging technique [21,22,23], which does not capture the three-dimensional data instantly, but fuses parts of the imaged volume over a period of several heart beats (~7 beats). Thus, the statistics are completely different for this kind of data. Furthermore, the contours in this data set appeared very much delineated and less effected by multiplicative speckle noise compared to US B-mode images captured with the same device. This leads us to the assumption, that also the internal preprocessing steps differ from the standard situation of two-dimensional data.

A possible extension of the proposed model in Section2 would consider an adapted version of the discriminant analysis described in this work. In particular, one could exchange the definition of the intraclass variances in (11) by weighted variants, i.e.,

$$\sigma_0^2(t) = \sum_{i=0}^{t} p_i \frac{\left(i - m_0(t)\right)^2}{m_0(t)}, \sigma_1^2(t) = \sum_{i=t+1}^{255} p_i \frac{\left(i - m_1(t)\right)^2}{m_1(t)}. \quad (17)$$

This adaption is motivated by the observation of different signal distribution variances depending on the unbiased signal intensity (cf. Loupas noise model [5, 6, 7, 8, 10]). First experiments showed an improvement for the estimation of an optimal threshold t_O as discussed in Section2.

However, the overall segmentation performance degraded by using this modified threshold in our segmentation formulation in (14). The reason for this is that the new threshold led in some cases to the fact, that speckle noise artifacts within the cavum of the left ventricle were wrongly classified as tissue region similar to the Chan-Vese method in Figure 6c. Thus, further investigations are needed to adapt the proposed method to medical ultrasound data more explicitly.

5 References

[1]. A Variational Framework for Region-Based Segmentation Incorporating Physical Noise Models by Alex Sawatzky, Daniel Tenbrinck, Xiaoyi Jiang, Martin Burger [December 2012]

[2]. Speckle Noise Reduction in Medical Ultrasound Images by Faouzi Benzarti, Hamid Amiri

[3]. E. Brown, T. Chan, and X. Bresson, Completely Convex Formulation of Bibliography 259 the Chan-Vese Image Segmentation Model, International Journal of Compututer Vision, 98 (2012), pp. 103–121. 59, 66, 84, 125

[4]. T. Chan and L. Vese, Active Contours Without Edges, IEEE Transactions on Image Processing, 10 (2001), pp. 266–277. 59, 65, 66, 67, 79, 82, 105, 112, 124, 125, 126, 128, 129, 134, 187

[5]. P. Coup´e, P. Hellier, C. Kevrann, and C. Barillot, Non-Local Meansbased Speckle Filtering for Ultrasound Images, IEEE Transactions on Image Processing, 18 (2009), pp. 2221–2229. 43, 46, 47

[6]. F. de Fontes, G. Barroso, P. Coup´e, and P. Hellier, Real Time Ultrasound Image Denoising, Journal of

Real-Time Image Processing, 6 (2011), pp. 15– 22. 43, 47

[7]. Z. Jin and X. Yang, A Variational Model to Remove the Multiplicative Noise in Ultrasound Images, Journal of Mathematical Imaging and Vision, 39 (2011), pp. 62–74. 43, 47, 68

[8]. T. Loupas, W. N. McDicken, and P. L. Allan, An Adaptive Weighted Median Filter for Speckle Suppression in Medical Ultrasonic Images, IEEE Transactions on Circuits and Systems, 36 (1989), pp. 129–135. 43, 47

[9]. N. Otsu, A Threshold Selection Method from Gray-Level Histograms, IEEE Transactions on Systems, Man, and Cybernetics, 9 (1979), pp. 62–66. 55, 131, 132, 133

[10]. L. Rudin, P.-L. Lions, and S. Osher, Geometric Level Set Methods in Imaging, Vision, and Graphics, Springer, 2003, ch. Multiplicative Denoising and Deblurring:Theory and Algorithms, pp. 103–119. 43, 46, 68

[11]. D. Tenbrinck and X. Jiang, Discriminant Analysis based Level Set Segmentation for Ultrasound Imaging, in Proceedings of the International Conference on Computer Analysis of Images and Patterns - CAIP, 2013, p. in press. 131, 185

[12]. D. Boukerroui, A Local Rayleigh Model with Spatial Scale Selection for Ultrasound Image Segmentation, in Proceedings of the British Machine Vision Conference - BMVC, 2012, pp. 84.1–84.12. 43, 46, 51, 62, 67, 68, 69, 100, 105

[13]. C. Li, C. Xu, C. Gui, and M. Fox, Level Set Evolution without Re- Initialization: A New Variational Formulation, in Proceedings of the International Conference on Computer Vision and Pattern Recognition - CVPR, 2005, pp. 430–

[14]. A. Sarti, C. Corsi, E. Mazzini, and C. Lamberti, Maximum Likelihood Segmentation of Ultrasound Images with RayleighDistribution, IEEE Transactions on Ultrasonics, Ferroelectrics and Frequency Control, 52 (2005), pp. 947–960. 43, 46, 62, 68, 69, 105

[15]. M. Tur, K. C. Chin, and J. W. Goodman, When is Speckle Noise Multiplicative?, Applied Optics, 21 (1982), pp. 1157–1159. 46

[16]. S. Osher and R. Fedkiw, Level Set Methods and Dynamic Implicit Surfaces, Springer Verlag, 2003. 58, 107, 108, 109, 111, 112, 113, 114, 115, 116, 117, 118, 119, 120, 121, 129, 142, 188

[17]. M. Sussman, P. Smereka, and S. Osher, A Level Set Approach for Computing Solutions to Incompressible Two-Phase Flow, Journal of Computational Physics, 114 (1994), pp. 146–159. 105, 121

[18]. J. Hegemann, Efficient Evolution Algorithms for Embedded Interfaces: From Inverse Parameter Estimation to a Level Set Method for Ductile Fracture, PhD thesis, University of M¨unster, July 2013. 105, 120

[19]. D. Mumford and J. Shah, Optimal Approximations by Piecewise Smooth Functions and Associated Variational Problems, Communications on Pure and Applied Mathematics, 42 (1989), pp. 577—-685. 58, 59, 63, 64, 66, 79, 80, 82

[20]. J. Strikwerda, Finite Difference Schemes and Partial Differential Equations, SIAM, 2004. 115, 118, 120, 127, 135

[21]. F. Flachskampf, Praxis der Echokardiografie, Thieme, 2010. 34, 36, 37, 42, 46, 202

[22]. C. Otto, Textbook of Clinical Echocardiography, Saunders, 2000. 35, 36, 37, 38, 39, 40, 41, 42, 48, 90, 91

[23]. G. Sutherland, L. Hatle, P. Claus, J. D'hooge, and B. Bijnens, eds., Doppler Myocardial Imaging, BSWK, 2002. 35, 36, 38, 39, 41, 42

[24]. W. Alt, Lineare Functionalanalysis, Springer Verlag, 1992. 14, 20, 21, 23, 24, 25,125, 154, 155

[25]. Image Segmentation Using the Chan-Vese Algorithm by Robert Crandall [Fall 2009 (http://math.arizona.edu/~rcrandall/ECE532_ProjectPaper.pdf)]

[26]. Anisotropic Diffusion of Ultrasound Constrained by Speckle Noise Model Karl Krissian, Kirby Vosburgh, Ron Kikinis and Carl-Fredrik Westin[Laboratory of Mathematics in Imaging, October 2004]

[27]. Chan–Vese Segmentation by Pascal Getreuer [Published in Image Processing On Line on 2012–08–08(Submitted on 2012–00–00, accepted on 2012–00–00.)]